DC Link Voltage Balancing of the Active Front-End for the Extreme Fast Charging Stations

Amirhossein Moeini
ECE Department
Missouri S&T
Rolla, Missouri, USA
amoeini@mst.edu

Sai Hemanth Kankanala
ECE Department
Missouri S&T
Rolla, Missouri, USA
skkcg@mst.edu

Jonathan W. Kimball
ECE Department
Missouri S&T
Rolla, Missouri, USA
kimballjw@mst.edu

***Abstract*—One of the most important challenges of the extreme fast charging (XFC) stations is to balance the DC link voltages of the active front-end (AFE). The multilevel cascaded H-bridge (CHB) converter is a great topology for the AFE applications due to the high power density, low total harmonic distortion (THD), and a low number of active and passive components. In this paper, a technique is proposed for balancing DC-link capacitor voltages of a three-phase CHB converter, when a phase shift-PWM modulation technique is used on all cells of the converter. To reach this goal, the redundant states of the CHB converters are used for generating different AC voltage levels by sorting the voltages of the converters. The proposed voltage balancing technique uses the principles that are employed for the DC link voltage balancing of the low-frequency modulation techniques to balance the DC link voltages of the CHB converter. As shown in this paper, the DC link voltages of the CHB converter can accurately be balanced very fast without using PI controllers, which are used in the conventional DC link voltage balancing techniques. A controller also is proposed which will be used to control the dq currents of the CHB converter. To verify the advantages of the proposed technique, the simulation results of the proposed technique will be carried out in a three-phase 7-cell CHB AFE.**

***Index Terms*—Grid-tied converters, cascaded H-bridge, DC link voltage balancing, fast charging station**

I. Introduction

Extreme fast charging (XFC) gains huge attention these days for the modern electric vehicles [1]–[6]. Multilevel converters have been used more and more these days due to their advantages, e.g., lower harmonics, higher voltage/power level, and modular structure [7] in the XFC applications. The main multilevel converters that are used in the industry are the cascaded H-bridge (CHB), neutral point clamped (NPC), and flying capacitors (FC) [7], [8]. Among them, the CHB converter has a higher power density, lower total harmonic distortion (THD), and a lower number of active and passive components [7], [9].

Extreme fast-charging stations (XFC) are necessary for the superfast charging of the electric vehicles. Each XFC requires an active front-end (AFE) when the grid is connected to the converter. Different power electronic topologies can be used for the AFE of the XFC [10]. The cascaded H-bridge (CHB) topology is a great option for the AFE of the XFC applications. The CHB converter can transfer high power to the EV loads and have low power losses due to the lower voltage on the DC side of the converters. However, one of the critical issues of the CHB converter is how to balance the DC link voltages of the AFE [11]. If the DC link voltages are not balanced or the references are not tracked, the controller cannot control the active and reactive power, current harmonic requirements cannot meet the power quality standards, and faults on the solid-state devices are inevitable.

Some of the main challenges of the CHB converters are to improve the speed of balancing of the DC link voltages, reduce the values of the passive filters, improve the controller performance of the CHB converters, and find accurate modeling of the CHB converters to analyze the reliability and controllability of the CHB converter. Also, meeting the power quality requirements of the different standards is another challenge of the CHB converters in industries [12].

In [7], [13], a technique was proposed to meet the requirements of the power quality standards for both voltages and currents at the point of common couplings (PCC) by using the low-frequency modulation techniques. In [11], a new technique was proposed to control the powers of the cells of the CHB converter without using DC link voltage sensors.

Several papers proposed techniques based on using PI controllers for the CHB by balancing the DC link voltages of the AFE with the PI controllers [14], [15]. However, using PI controllers increase the delays of balancing the DC link voltages. In [16], a new technique was proposed based on using the redundant states of the CHB converter for balancing the DC link voltages, when the low-frequency modulation technique (selective harmonic elimination-PWM) are used. In [17], a technique was proposed to balance the DC link voltages of the AFE based on the redundant states of the converter. However, the technique in [17] cannot balance the DC link voltages for any active or reactive power that is desirable. Moreover, the implementation of the voltage balancing technique in [17] is complicated for sorting the voltages of decoupling capacitors when a high number of H-bridge cells are used. Furthermore, the speed of voltage balancing technique in [17] is not as high as possible due to considering the instantaneous power of the converter at

This work was supported by the U.S. Department of Energy, under Grant DE-EE0008449

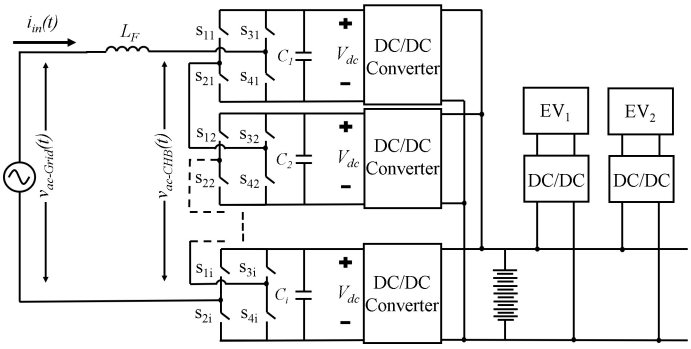

Fig. 1. Configuration of a single-phase CHB grid-tied converter for EV charging stations.

the PCC. In [18], a technique based on the sorting of the DC voltages of the CHB converters was proposed to balance the DC link voltages of the CHB converter with the high-switching frequency level shift-PWM modulation technique. However, the technique in [18] does not apply to other high-switching frequency modulation techniques. In this paper, a DC link voltage balancing technique will be proposed for the AFE based on the available redundant states of the CHB converter for generating different voltage levels. The proposed technique work for any values of the active and reactive powers due to using the instantaneous power that is injected into the CHB converter. Furthermore, to balance the DC link voltages of the CHB converter, the voltages of the H-bridge cells are sorted before applying each switching state to the cells of the converter. Furthermore, the proposed technique in this paper can be employed in any low- or high-switching frequency modulation techniques.

The paper is organized as follows; Section II discusses about the derived fundamental equations of the CHB converters. Section III proposes the new DC link voltage balancing technique and how to simply sort and implement the DC link voltage balancing technique. Moreover, section IV illustrates the simulation results to validate the advantages of the proposed technique. Finally, section V concludes the paper.

II. Configuration of the Cascaded H-Bridge Converter for the Active Front-End

The configuration of one phase of the AFE topology is shown in Fig. 1. As shown in Fig. 1, the CHB converter is connected to the grid by using the coupling inductance L_F. $v_{(ac-CHB)}(t)$, $v_{(ac-Grid)}(t)$, and $i_{in}(t)$ are the AC CHB voltage of the converter, the AC grid voltage, and the AC input current of the converter for a single-phase AFE, respectively. As shown in Fig. 1, i number of cells of H-bridges are connected to the DC/DC converters to supply energy to the EVs. The AC side equation of a three phase AFE can be written as,

TABLE I
Odd order current harmonic requirements of the IEEE Std. 519 [19] at the point of common coupling (PCC)

Harmonic order	Current limit
$1 < h < 11$	4%
$11 \leq h < 17$	2%
$17 \leq h < 23$	1.5%
$23 \leq h < 35$	0.6%
$35 \leq h < 50$	0.3%
TDD	5%

$$\begin{cases} v_{(ac-Grid-phase-A)}(t) = L_F \frac{di_{(in-phase-A)}(t)}{dt} \\ \quad +v_{(ac-CHB-phase-A)}(t), \\ v_{(ac-Grid-phase-B)}(t) = L_F \frac{di_{(in-phase-B)}(t)}{dt} \\ \quad +v_{(ac-CHB-phase-B)}(t), \\ v_{(ac-Grid-phase-C)}(t) = L_F \frac{di_{(in-phase-C)}(t)}{dt} \\ \quad +v_{(ac-CHB-phase-C)}(t). \end{cases} \tag{1}$$

where $v_{(ac-Grid-phase-A)}(t)$, $v_{(ac-Grid-phase-B)}(t)$, $v_{(ac-Grid-phase-A)}(t)$ are the three phase grid voltages. Also, $v_{(ac-CHB-phase-A)}(t)$, $v_{(ac-CHB-phase-B)}(t)$, and $v_{(ac-CHB-phase-A)}(t)$ are the three phase CHB voltages. Moreover, $i_{(in-phase-A)}(t)$, $i_{(in-phase-B)}(t)$, and $i_{(in-phase-C)}(t)$ are the injected three phase currents of the converter. The three-phase equations of the CHB converter in the Laplace domain are

$$\begin{cases} V_{(ac-Grid-phase-A)}(s) = sL_F I_{(in-phase-A)}(s) \\ \quad +V_{(ac-CHB-phase-A)}(s), \\ V_{(ac-Grid-phase-B)}(s) = sL_F I_{(in-phase-B)}(s) \\ \quad +V_{(ac-CHB-phase-B)}(s), \\ V_{(ac-Grid-phase-C)}(s) = sL_F I_{(in-phase-C)}(s) \\ \quad +V_{(ac-CHB-phase-C)}(s), \end{cases} \tag{2}$$

$V_{(ac-Grid-phase-A)}$, $V_{(ac-Grid-phase-B)}$, and $V_{(ac-Grid-phase-C)}$ are the three-phase grid voltage vectors. $V_{(ac-CHB-phase-A)}$, $V_{(ac-CHB-phase-B)}$, and $V_{(ac-CHB-phase-C)}$ are the three-phase CHB voltage vectors. Moreover, $V_{(ac-CHB-phase-A)}$, $V_{(ac-CHB-phase-B)}$, and $V_{(ac-CHB-phase-C)}$ are the three-phase AC current vectors. The dq time-domain components of the the injected current of the converter to the grid are found from

$$\begin{cases} v_{(ac-Grid-d)}(t) = L_F \frac{di_{(in-d)}(t)}{dt} - \omega L_F i_{(in-q)}(t) \\ \quad +v_{(ac-CHB-d)}(t), \\ v_{(ac-Grid-q)}(t) = L_F \frac{di_{(in-q)}(t)}{dt} + \omega L_F i_{(in-d)}(t) \\ \quad +v_{(ac-CHB-q)}(t). \end{cases} \tag{3}$$

where, $v_{(ac-Grid-d)}(t)$ and $v_{(ac-Grid-q)}(t)$ are the d and q components of the AC grid voltage, respectively. Also, $v_{(ac-CHB-d)}(t)$ and $v_{(ac-Grid-q)}(t)$ are the d and q components of the AC CHB voltage, respectively. In the simulation, by using the ABC to dq transformation, the dq components of the CHB voltage, the grid voltage, and the AC current of

the converter are calculated. The controller, which is used in this paper to control the CHB converter, is shown in Fig. 2. As shown in Fig. 2, the DC link voltages of the CHB converter are averaged and compared with V_{dc-ref}. The error signal is applied to a proportional-integral (PI) controller to find the reference d component current ($I_{(in-d-ref)}$) as shown in Fig. 2. Moreover, the reference q component current can be designed to compensate the injected reactive current of the converter. Then, based on the equation (3), the references of the dq components of the CHB voltage are selected. To decouple dq voltages of the CHB from the qd components of current in (3), d and q components of AC current are multiplied with ωL_F and feed-forwarded in the q and d components of the CHB voltage as shown in Fig. 2. The PI controllers also control the dq voltages of the CHB converter to track the references dq currents of the AFE. Moreover, based on the equation (3), the dq components of the grid voltage ($V_{(ac-Grid-d)}$ and $V_{(ac-Grid-q)}$) are feed-forwarded in Fig. 2. Thus, the voltage of the converter are controlled from the equation (3). The grid-tied converter must meet the power quality standards at the point of common coupling (PCC). An example of the power quality standard, that is required to meet, is shown in Table I. In this table, TDD is the total demand distortion [19]. h is the harmonic order. The Table I is obtained when the $\frac{I_{sc}}{I_L} \leq 20$, where I_{sc} and I_L are the short circuit current and the load current of the CHB converter at the PCC, respectively. To meet the requirements of IEEE Std. 519, the following equations must be met by the three-phase CHB converter.

$$\begin{cases} \left| \frac{I_{(in-phase-A-h)}}{I_L} \right| = \\ \left| \frac{V_{(ac-Grid-phase-A-h)} - V_{(ac-CHB-phase-A-h)}}{h\omega L_F I_L} \right| \leq C_h, \\ \left| \frac{I_{(in-phase-B-h)}}{I_L} \right| = \\ \left| \frac{V_{(ac-Grid-phase-B-h)} - V_{(ac-CHB-phase-B-h)}}{h\omega L_F I_L} \right| \leq C_h, \\ \left| \frac{I_{(in-phase-C-h)}}{I_L} \right| = \\ \left| \frac{V_{(ac-Grid-phase-C-h)} - V_{(ac-CHB-phase-C-h)}}{h\omega L_F I_L} \right| \leq C_h. \end{cases} \tag{4}$$

where $I_{(in-phase-A-h)}$, $I_{(in-phase-B-h)}$, and $I_{(in-phase-C-h)}$ are the three-phase AC injected current of the converter for the hth order harmonic. Moreover, $V_{(ac-CHB-phase-A-h)}$, $V_{(ac-CHB-phase-B-h)}$, and $V_{(ac-CHB-phase-C-h)}$ are the three-phase AC CHB voltages of the converter for the hth order harmonic. Finally, $V_{(ac-Grid-phase-A-h)}$, $V_{(ac-Grid-phase-B-h)}$, and $V_{(ac-Grid-phase-C-h)}$ are the three-phase AC grid voltages of the converter for the hth order harmonic.

The modulation technique which will be used in this paper is the phase-shift-PWM (PS-PWM) technique [12], which is a kind of the high-switching frequency modulation techniques. The main principle of the PS-PWM technique is to compare the reference signal with the triangle or the saw-tooth waveform with a high carrier frequency to generate the signals of the power electronic switches. For the CHB converter, the output voltage of the CHB converter must be calculated for each harmonic order by using

$$\begin{cases} \left| \frac{I_{(in-phase-A-h)}}{I_L} \right| = \\ \left| \frac{V_{(ac-Grid-phase-A-h)} - V_{(ac-CHB-phase-A-h)}}{h\omega L_F I_L} \right| \leq C_h, \\ \left| \frac{I_{(in-phase-B-h)}}{I_L} \right| = \\ \left| \frac{V_{(ac-Grid-phase-B-h)} - V_{(ac-CHB-phase-B-h)}}{h\omega L_F I_L} \right| \leq C_h, \\ \left| \frac{I_{(in-phase-C-h)}}{I_L} \right| = \\ \left| \frac{V_{(ac-Grid-phase-C-h)} - V_{(ac-CHB-phase-C-h)}}{h\omega L_F I_L} \right| \leq C_h. \end{cases} \tag{5}$$

For each phase of the CHB converter, the CHB converter will generate a voltage waveform based on the modulation technique that is used. In this paper, the high-switching frequency phase-shift PWM (PS-PWM) modulation technique is used. The main principle of the PS-PWM technique is to compare the reference of the AC voltage with a triangle waveform which has an initial carrier frequency of ω_c and an initial phase of θ_c. The fundamental and harmonics of the PS-PWM technique are

$$\begin{aligned} v_{(ac-CHB-PSPWM)}(t) &= iV_{dc}M\cos(\omega_0 t + \theta_0) \\ &+ \frac{4V_{dc}}{\pi} \sum_{B=1}^{\infty} \sum_{A=-\infty}^{\infty} \begin{pmatrix} \frac{1}{2B} J_{2A-1}(iB\pi M) \times \\ \sin((2iB + 2A - 1)\frac{\pi}{2}) \times \\ \cos(2iB\omega_c t + (2A-1)(\omega_0 t + \theta_0)) \end{pmatrix} \end{aligned} \tag{6}$$

where, $v_{(ac-CHB-PSPWM)}(t)$ is the time-domain voltage of the CHB converter with the PS-PWM technique. Furthermore, i is the number of cells of the CHB converter that has the PS-PWM modulation technique. Also, A and B are the side-band and base-band harmonics of the CHB converter. Moreover, J is the Bessel function of the first kind. M is the average of the modulation index of i-cell of the CHB converter. If the total modulation index of the CHB converter is M_a, M is found by using $M = \frac{M_a}{i}$. As shown in Fig. 3, the PS-PWM technique has several base-band harmonics. Moreover, around each base-band harmonic, there exist several side-band harmonics. From the equation (6), the number of these side-band harmonics of each based-band harmonic is infinity. However, beyond a certain bandwidth, the sideband harmonics are small and may be ignored. For baseband harmonic B, the bandwidth is,

$$BW_B \approx 2(iMB\pi + 2)f_0. \tag{7}$$

The CHB converter generates the following redundant voltage states (Table II) for different voltage levels, if just two cells are used and the redundant states that increase the switching transitions of the converter are ignored (e.g., cell # 1=$+V_{dc}$ and cell # 2=$-V_{dc}$ for generating the zero voltage level, etc). Table II can be extended for any number of cells of the CHB converter. Table II shows that for generating different voltage levels of the CHB converter, the redundant states must be used to balance the DC link voltages of the converter. There exists

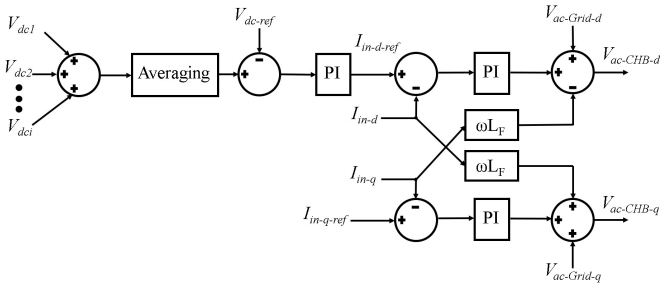

Fig. 2. Controller of a three-phase CHB grid-tied converter for EV charging stations.

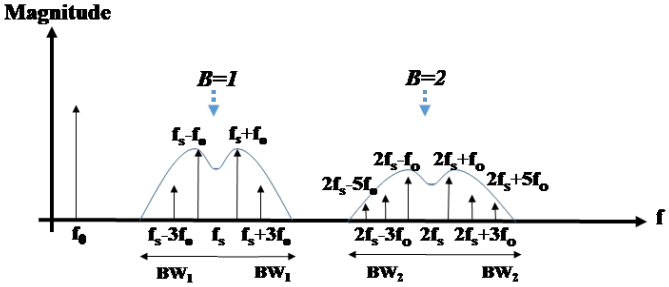

Fig. 3. Harmonic envelope of the PS-PWM technique.

TABLE II
REDUNDANT STATES OF THE CHB CONVERTER FOR GENERATING DIFFERENT VOLTAGE LEVELS WITH A 2-CELL CHB CONVERTER.

voltage level	cell # 1	cell # 2
$+2V_{dc}$	$+V_{dc}$	$+V_{dc}$
$+V_{dc}$	$+V_{dc}$	0
$+V_{dc}$	0	$+V_{dc}$
0	0	0
$-V_{dc}$	$-V_{dc}$	0
$-V_{dc}$	0	$-V_{dc}$
$-2V_{dc}$	$-V_{dc}$	$-V_{dc}$

an equation for the number of available redundant states of the CHB converter for all cells. As can be inferred from Table II, the number of available states for each voltage level of the CHB converter is

$$NS_j = \binom{i}{|j|} \tag{8}$$

where, NS_j is the number of available redundant states of the jth voltage level of the CHB converter. From 8, due to using the absolute value for j, similar to the positive voltage levels, the negative voltage levels also generate the same number of redundant states. Using (8) to sum all available redundant states of the CHB converter for both positive and negative voltages, the total number of states that are available for an i-cell CHB grid-tied converter is obtained based on the following equation,

$$TNS = 2\left(\binom{i}{0} + \binom{i}{1} + \ldots + \binom{i}{i}\right) - 1 = 2^{i+1} - 1. \tag{9}$$

where TNS is the total number of states of the i-cell CHB converter. The minus one (-1) in (9) is due to counting the zero voltage level once during counting the total number of available redundant states of the CHB converter.

Equation (9) proves that having a higher number of cells of H-Bridges in an AFE will exponentially increase the number of redundant states. This increases the number of lines of code that are needed to implement the proposed voltage balancing technique in simulations and experiments. Thus, the proposed technique in this paper is suitable for use on the applications which require a low number of cells of the CHB converter. The details on how to implement the negative and positive switchings to not increase the lines of code in simulations and experiments are shown in Algorithm 1.

III. Proposed DC-Link Voltage Balancing Technique for High-Switching Frequency Modulation Techniques

In the proposed voltage balancing technique, the redundant states that are available for the CHB converter as shown in Table II and equation (9) are used for balancing the DC link voltages of the CHB converter. To reach this goal, first, the voltage level of the CHB converter must be evaluated. In the low-frequency modulation technique, the predefined waveform of the CHB converter will be used to find the voltage level of the CHB converter. For the high-switching frequency modulation technique, e.g., phase-shift PWM (PS-PWM), based on the switching states that are applied to the switches of the converter, the voltage level of the converter at each time instant is obtained as shown in equation (9),

$$V_L = S_{11} - S_{31} + S_{12} - S_{32} + \ldots + S_{1i} - S_{3i}. \tag{10}$$

where, V_L is the voltage level of the CHB converter, S_{1k} and S_{3k} are the gate signals of the kth cell of the CHB converter for the first and the third switches in Fig. 1. The gate signals (S_{1k} and S_{3k}), which are obtained from the modulation block of the controller, have binary values (0 for off and 1 for on states). Using (10), the voltage level of the CHB converter before applying each switching state to the cells of the converter is obtained.

Next, the instantaneous powers that are injected to the three-phase CHB converter in 2 must be checked for the proposed DC-link voltage balancing technique. The injected instantaneous powers of three-phase CHB converter are calculated as

$$\begin{cases} p_{(inst-phase-A)}(t) = & v_{(ac-CHB-phase-A)}(t) \\ & \times i_{(in-phase-A)}(t), \\ p_{(inst-phase-B)}(t) = & v_{(ac-CHB-phase-B)}(t) \\ & \times i_{(in-phase-B)}(t), \\ p_{(inst-phase-C)}(t) = & v_{(ac-CHB-phase-C)}(t) \\ & \times i_{(in-phase-C)}(t), \end{cases} \tag{11}$$

TABLE III
PROPOSED VOLTAGE BALANCING TECHNIQUE BY USING REDUNDANT STATES OF TWO-CELL OF THE CHB CONVERTER.

V_L	relationship	sign of power	cell # 1	cell # 2
$+V_{dc}$	$V_{dc1} \leq V_{dc2}$	$+$	$+V_{dc}$	0
$+V_{dc}$	$V_{dc2} \leq V_{dc1}$	$+$	0	$+V_{dc}$
$+V_{dc}$	$V_{dc1} \leq V_{dc2}$	$-$	0	$+V_{dc}$
$+V_{dc}$	$V_{dc2} \leq V_{dc1}$	$-$	$+V_{dc}$	0
$-V_{dc}$	$V_{dc1} \leq V_{dc2}$	$+$	$-V_{dc}$	0
$-V_{dc}$	$V_{dc2} \leq V_{dc1}$	$+$	0	$-V_{dc}$
$-V_{dc}$	$V_{dc1} \leq V_{dc2}$	$-$	0	$-V_{dc}$
$-V_{dc}$	$V_{dc2} \leq V_{dc1}$	$-$	$-V_{dc}$	0
$+2V_{dc}$	-	-	$+V_{dc}$	$+V_{dc}$
$-2V_{dc}$	-	-	$-V_{dc}$	$-V_{dc}$
0	-	-	0	0

where $p_{(inst-phase-A)}(t)$, $p_{(inst-phase-B)}(t)$, and $p_{(inst-phase-C)}(t)$ are the instantaneous powers that flow through the A, B, and C phases for the CHB converter, respectively.

Table III shows the proposed DC link voltage balancing technique that is used for any modulation techniques. Table III shows that by measuring the DC link voltages of each phase of the converter and the sign of the instantaneous power that is injected to a phase of the converter, the switching transitions of the CHB converter can be selected, which balance the DC link voltages of the converter. The controller block of the AFE that is used in the simulations is shown in Fig. 2. The controller in this figure controls the power, that is injected to all three-phases of the converter. However, the DC link voltages of the CHB cells cannot be controlled by using Fig. 2. To solve this issue, Algorithm 1 is used in this paper to balance the DC link voltages based on Table III. As shown in Algorithm 1, to reduce the required memory of the microprocessor, the proposed DC link voltage balancing technique uses the V_L to select the switching states of the converter. As shown in this algorithm, if the V_L is higher than 0, the exact AC output voltage of cells of the CHB that is obtained from Table III will be applied to the cells of the converter. However, if the V_L is lower than 0, the negative of the exact AC voltage of cells of the CHB that is obtained from Table III will be applied to the cells of the converter. Moreover, in the Algorithm 1, the DC link voltages are stored in the memory of the microprocessor when the voltage level of the CHB is changed by the modulation technique.

IV. SIMULATION RESULTS OF THE PROPOSED TECHNIQUE

Parameters of the simulation results in this paper are shown in Table IV. In the simulation results, a full load condition, which is shown in Table IV, is investigated for a three-phase 7-cell CHB converter. The PLECS software is used for obtaining the simulation results in this paper. Fig. 4 shows the time-domain waveforms of the grid-tied CHB converter for the full load condition. In Fig. 4, the q component current is equal to zero. Moreover, the d component current is equal to the power that is controlled based on the controller in Fig. 2 to balance the DC link voltages around (200V). Fig. 4(a) shows the three

Algorithm 1 The proposed DC link voltage balancing pseudo-code.

1. Measure all DC link voltages of the CHB converter in each phase.
2. Check the voltage level of the time-domain waveform of the CHB converter based on (10).
3. Save data of the DC link voltages at the time instant that the voltage level is changed.
4. Compare and sort the DC link voltages to select the best switching transitions based on Table III.
5. Check the voltage level:
if $V_L > 0$ **then**
| Generate the cells' voltage based on Table III,
else
| Generate an inverse of the cells' voltage based on Table III.
end

TABLE IV
PARAMETERS OF THE CHB CONVERTER DURING THE SIMULATION RESULTS.

Parameter	Symbol	Value
AC grid voltage	$V_{(ac-Grid)}$	1050V
grid frequency	f	60Hz
rated power	$P_{nominal}$	30kW
grid inductance	L_F	0.054pu
DC link voltage	$V_{(dc-ref)}$	200V
number of cells	i	7

phase voltages of the grid $v_{(ac-Grid)}(t)$. Moreover, Fig. 4(b) shows the time-domain waveform of the three-phase CHB voltages $v_{(ac-CHB)}(t)$. Also, Fig. 4(c) shows the time-domain waveform of the current that is injected to the grid. As shown in this figure, the ripples of the AC current in the three-phases are negligible. Thus, the harmonics and TDD of the current are low. This is due to the fact that the converter uses a high-switching frequency modulation technique and the coupling inductance which has a great role in meeting the requirements of the IEEE Std. 519 standard in (5). Furthermore, Fig. 5 shows the time-domain waveform of the 7-cell H-bridge voltages that use the proposed voltage balancing technique in this paper. As shown in this paper, the proposed technique controls 7-cells of H-bridges to the reference voltage (200V) within 0.1s without using any PI controllers for balancing the DC link voltages. As shown, the ripples of the proposed technique are small. Fig. 6 shows the simulation results of the proposed voltage balancing technique, when the reactive current at the PCC is equal to 30A and the active power is equal to the active current is selected from the controller of the DC link voltages of the CHB based on the Fig. 2, when the load of the EV is 120kW. Fig. 6(a) shows the time-domain waveform of the grid voltage. Moreover, Fig. 6(b) illustrates the CHB voltage of three-phases. Furthermore, Fig. 6(c) shows the three-phase injected current of the grid-tied converter. As shown in this figure, the ripples of the current again are low due to the high switching frequency of the converter and the high value of the coupling inductance of the converter.

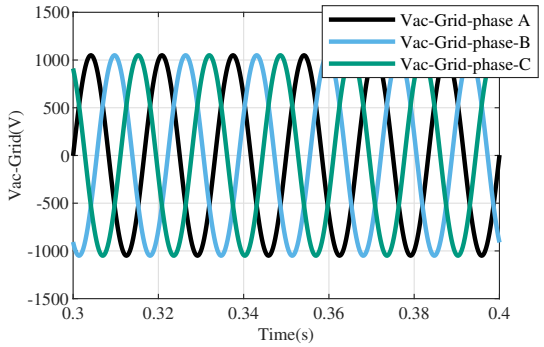

(a)

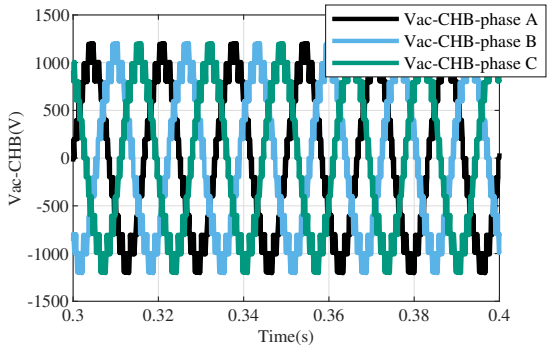

(b)

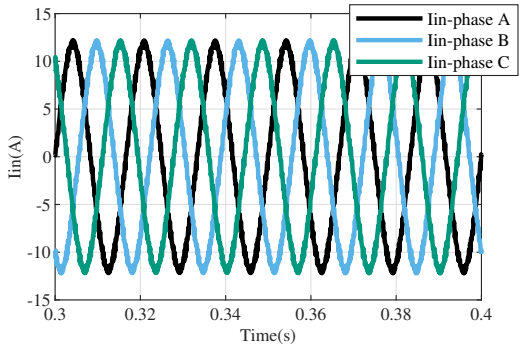

(c)

Fig. 4. Simulation results of the time-domain waveforms for the three-phase grid-tied CHB converter, (a) time-domain waveforms of the $v_{(ac-Grid)}(t)$ (b) time-domain waveforms of the $v_{(ac-CHB)}(t)$, (c) time-domain waveforms of the $i_{in}(t)$.

Thus, the harmonics and the TDD of the converter meet the requirements of the power quality standard. Moreover, Fig. 7 shows the DC link voltages of the grid-tied converter, when I_q is equal to 30A and the active current is selected from the controller of the DC link voltages of the CHB based on the Fig. 2, when the load of the EV is 120kW. As shown in this figure, the proposed technique controls the DC link voltages to the reference voltage (200V) for four-quadrant active and reactive power.

To prove the advantages of the proposed technique during the dynamic condition, when the reactive or active power is changed, a dynamic analysis is done in Fig. 8. The simulation of the Fig. 8 shows the simulation results of the proposed

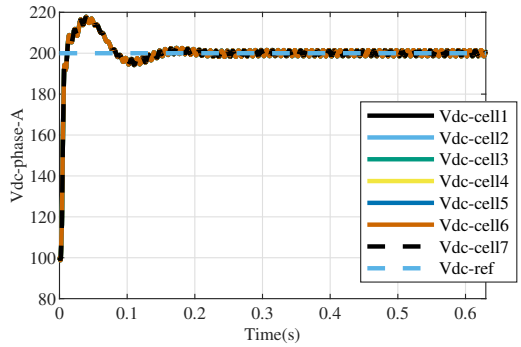

Fig. 5. DC link voltages of the phase A of a three-phase CHB grid-tied converter.

voltage balancing technique during dynamic conditions when the reactive current at the PCC is changed from 30A to -30A and the active current is selected from the controller of the DC link voltages of the CHB based on the Fig. 2, when the load of the EV is 120kW at t=0.15s. Fig. 8(a) shows the time-domain waveform of the grid voltage. Moreover, Fig. 8(b) illustrates the CHB voltage of three-phases of the converter. Furthermore, Fig. 8(c) shows the three-phase injected AC current of the grid-tied converter. Thus, AC current harmonics and TDD of the CHB converter are small due to the high switching frequency of the converter and the high coupling inductance of the converter. Moreover, in this figure, due to not changing the reactive power at $\theta = \frac{\pi}{2}$, the transient response is generated in the time-domain waveform of the current of the converter as discussed in [20]. Moreover, Fig. 9 shows the DC link voltages of the grid-tied converter during the transient, when I_q is changed from 30A to -30A. As shown in this figure, the proposed technique controls the DC link voltages to the reference voltage (200V) for the four-quadrant active and reactive power. Furthermore, the proposed DC link voltage balancing technique regulates the DC link voltages of the converter without significantly disturbing the DC link voltages. The reactive power is approximately dependent on the difference between the voltages of the grid and the CHB converter. While the active power is mainly controlled by changing the phase difference between the CHB voltage and the grid voltage. Thus, to change the active power, the voltage magnitude of the CHB converter will not be changed significantly or when the reference of the reactive power is changed, the phase difference of the CHB converter will not be changed drastically. As shown in this figure, having -30A reactive current requires a lower CHB voltage magnitude. To this end, a lower number of CHB cells will be involved in the transferred power. This also proves that for different reactive or active currents, the ripples of the DC link voltages are different.

V. Conclusion

In this paper, a voltage balancing technique was proposed for both low- and high-switching frequency modulation tech-

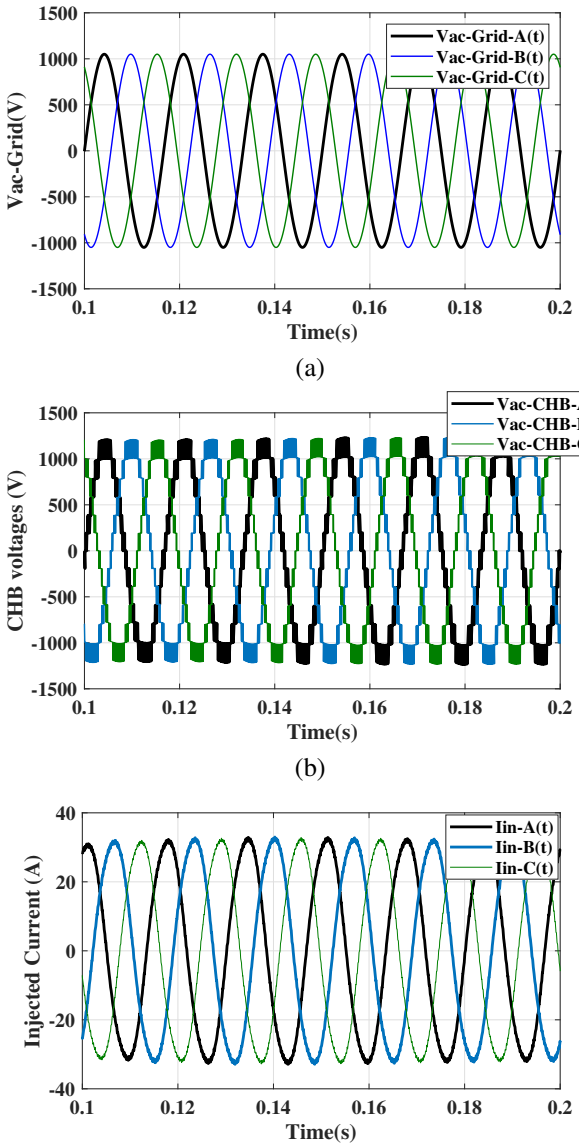

Fig. 6. Simulation results of the time-domain waveform for the three-phase grid-tied CHB converter when $I_{q-ref} = 30A$, (a) time-domain waveform of the $v_{(ac-Grid)}(t)$ (b) time-domain waveform of the $v_{(ac-CHB)}(t)$, (c) time-domain waveform of the $i_{in}(t)$.

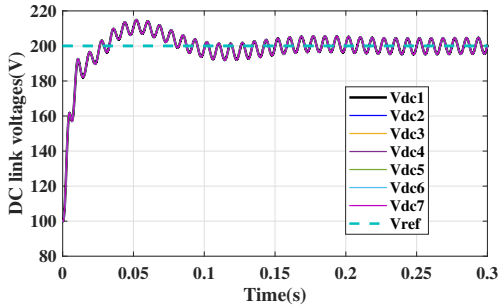

Fig. 7. DC link voltages of the phase A of the three-phase CHB grid-tied converter when $I_{q-ref} = 30A$.

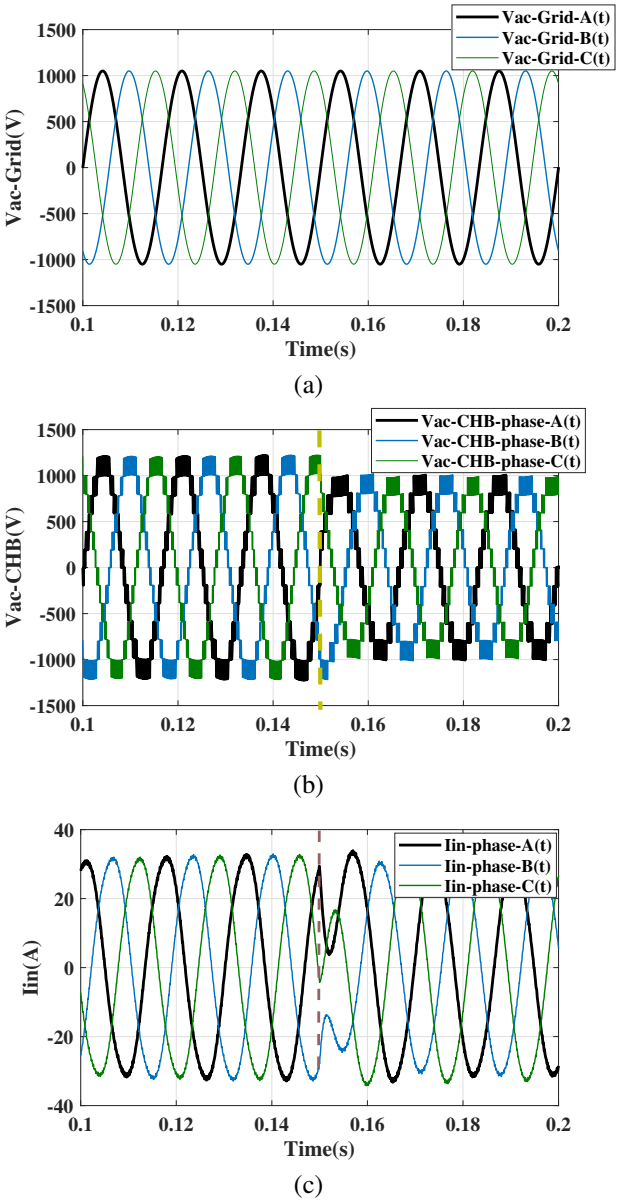

Fig. 8. Simulation results of the time-domain waveform for the three-phase grid-tied CHB converter when I_{q-ref} is changed from 30A to -30A at t=0.15s, (a) time-domain waveform of the $v_{(ac-Grid)}(t)$ (b) time-domain waveform of the $v_{(ac-CHB)}(t)$, (c) time-domain waveform of the $i_{in}(t)$.

niques of the CHB converter. As shown in the simulation results of this paper, the DC link voltages of the CHB converter could accurately be regulated for any number of cells by using the redundant states of the CHB converter. As proven in the simulation results, the proposed DC link voltage balancing technique balances the DC link voltages for any low- and high-frequency modulation techniques, when the current have any active and reactive currents. The dynamic response of the CHB converter also was shown to prove the advantages of the proposed DC link voltage balancing technique under dynamic conditions. As proven in the simulation results, without increasing the switching frequency of the CHB converter, the DC link voltages are accurately regulated under dynamic

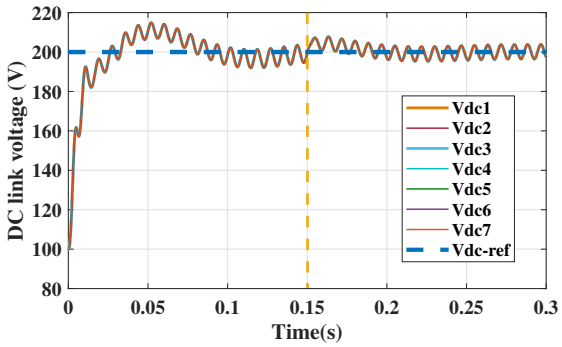

Fig. 9. DC link voltages of the phase A of the three-phase CHB grid-tied converter when I_{q-ref} is changed from 30A to -30A at t=0.15s.

conditions. In future work, the hardware implementation of the CHB converter with the proposed voltage balancing technique will be investigated. Also, some novel techniques to implement the proposed technique for a higher number of cells of the CHB converter will be implemented.

REFERENCES

[1] M. Dabbaghjamanesh, A. Moeini, and A. Kavousi-Fard, "Reinforcement learning-based load forecasting of electric vehicle charging station using q-learningtechnique," *IEEE Transactions on Industrial Informatics*, pp. 1–1, 2020.

[2] M. Dabbaghjamanesh, A. Kavousi-Fard, and J. Zhang, "Stochastic modeling and integration of plug-in hybrid electric vehicles in reconfigurable microgrids with deep learning-based forecasting," *IEEE Transactions on Intelligent Transportation Systems*, 2020.

[3] F. Ferdowsi, M. Dabbaghjamanesh, S. Mehraeen, and M. Rastegar, "Optimal scheduling of reconfigurable hybrid ac/dc microgrid under dlr security constraint," in *2019 IEEE Green Technologies Conference (GreenTech)*. IEEE, 2019, pp. 1–5.

[4] E. Taherzadeh, S. Javadi, and M. Dabbaghjamanesh, "New optimal power management strategy for series plug-in hybrid electric vehicles," *International Journal of Automotive Technology*, vol. 19, no. 6, pp. 1061–1069, 2018.

[5] E. Taherzadeh, M. Dabbaghjamanesh, M. Gitizadeh, and A. Rahideh, "A new efficient fuel optimization in blended charge depletion/charge sustenance control strategy for plug-in hybrid electric vehicles," *IEEE Transactions on Intelligent Vehicles*, vol. 3, no. 3, pp. 374–383, 2018.

[6] M. Dabbaghjamanesh, A. Moeini, J. Kimball, and J. Zhang, "Using gated recurrent units for selective harmonic current mitigation-pwm in grid-tied cascaded h-bridge converters," *IEEE Transactions on Industry Applications*, pp. 1–1, 2020.

[7] A. Moeini and S. Wang, "An asymmetric selective harmonic current and voltage modulation-PWM technique for electric vehicle charging stations with cascaded H-bridge converters to meet power quality standards," in *2019 IEEE Energy Conversion Congress and Exposition (ECCE)*, Sep. 2019, pp. 4395–4402.

[8] K. Yang, J. Hao, and Y. Wang, "Switching angles generation for selective harmonic elimination by using artificial neural networks and quasi-newton algorithm," in *2016 IEEE Energy Conversion Congress and Exposition (ECCE)*, Sep. 2016, pp. 1–5.

[9] M. Balasubramonian and V. Rajamani, "Design and real-time implementation of SHEPWM in single-phase inverter using generalized Hopfield neural network," *IEEE Transactions on Industrial Electronics*, vol. 61, no. 11, pp. 6327–6336, Nov 2014.

[10] L. G. Franquelo, J. Napoles, R. C. P. Guisado, J. I. Leon, and M. A. Aguirre, "A flexible selective harmonic mitigation technique to meet grid codes in three-level PWM converters," *IEEE Transactions on Industrial Electronics*, vol. 54, no. 6, pp. 3022–3029, Dec 2007.

[11] A. Moeini and S. Wang, "A dc link sensor-less voltage balancing technique for cascaded H-bridge multilevel converters with asymmetric selective harmonic current mitigation-PWM," *IEEE Transactions on Power Electronics*, vol. 33, no. 9, pp. 7571–7581, 2017.

[12] A. Moeini, S. Wang, B. Zhang, and L. Yang, "A hybrid phase shift-PWM and asymmetric selective harmonic current mitigation-PWM modulation technique to reduce harmonics and inductance of single-phase grid-tied cascaded multilevel converters," *IEEE Transactions on Industrial Electronics*, 2019.

[13] A. Moeini and S. Wang, "Analyzing and reducing current harmonics of ac and dc sides of cascaded H-bridge converters for electric vehicle charging stations," in *2019 IEEE Energy Conversion Congress and Exposition (ECCE)*, 2019, pp. 193–200.

[14] H. Akagi, S. Inoue, and T. Yoshii, "Control and performance of a transformerless cascade PWM STATCOM with star configuration," *IEEE Transactions on Industry Applications*, vol. 43, no. 4, pp. 1041–1049, July 2007.

[15] Y. Zhuang, C. Wang, C. Wang, H. Cheng, Y. Gong, and H. Wang, "Determination method for topology configuration of hybrid cascaded H-bridge rectifiers," 2016.

[16] A. Moeini and S. Wang, "A dc link sensor-less voltage balancing technique for cascaded H-bridge multilevel converters with asymmetric selective harmonic current mitigation-PWM," *IEEE Transactions on Power Electronics*, vol. 33, no. 9, pp. 7571–7581, Sep. 2018.

[17] H. Iman-Eini, J.-L. Schanen, S. Farhangi, and J. Roudet, "A modular strategy for control and voltage balancing of cascaded H-bridge rectifiers," 2008.

[18] H. Vahedi, M. Sharifzadeh, K. Al-Haddad, and B. M. Wilamowski, "Single-dc-source 7-level CHB inverter with multicarrier level-shifted PWM," in *IECON 2015 - 41st Annual Conference of the IEEE Industrial Electronics Society*, 2015, pp. 004 328–004 333.

[19] "IEEE recommended practice and requirements for harmonic control in electric power systems," *IEEE Std 519-2014 (Revision of IEEE Std 519-1992)*, pp. 1–29, June 2014.

[20] S. Wang, H. Zhao, and A. Moeini, "Control to output dynamic response and extend modulation index range with hybrid selective harmonic current mitigation-PWM and phase-shift PWM for four-quadrant cascaded H-bridge converters," Mar. 24 2020, uS Patent 10,601,305.